



Full length article

Focusing gain analysis of time-reversal precoding in MISO OFDM communication systems[☆]

Trung-Hien Nguyen^{a,*}, Jean-François Determe^a, Shaghayegh Monfared^a,
Jérôme Louveaux^b, Philippe De Doncker^a, François Horlin^a

^a OPERA department, Université libre de Bruxelles (ULB), 1050 Brussels, Belgium

^b ICTEAM institute, Université catholique de Louvain (UCL), 1348 Louvain-la-Neuve, Belgium



ARTICLE INFO

Article history:

Received 23 January 2020
Received in revised form 8 June 2020
Accepted 2 October 2020
Available online 6 October 2020

Keywords:

Time-reversal
Rate back-off factor
OFDM

ABSTRACT

Emerging communication systems can benefit from time-reversal (TR) technology thanks to its good spatio-temporal signal focusing effect. The recent advances in low-cost wideband devices fabrication further leverage the use of TR wideband communication systems. The TR is generally carried out in the time domain and the focusing effect of TR comes from the use of a high transmit rate back-off factor (BOF), which is the signal up-sampling rate. In spite of the widely-used orthogonal frequency-division multiplexing (OFDM) modulation, few works have investigated the frequency-domain (FD) TR precoding in combination with OFDM communication systems. Furthermore, most existing works on FD/TR precoding rely on multiple-antenna technology at the transmitter to create the focusing effect. In this paper, we investigate the focusing gain provided by TR precoding in multiple-input single-output (MISO) OFDM systems. In particular, we compare the communication performance of such system at the intended position and that at the unintended position. Based on the analysis, we demonstrate that increasing the BOF and/or the number of transmit antennas significantly improves the focusing effect at the intended position. In contrast, the unintended positions receive less useful power. We derive approximated mean-square-error (MSE) expressions of equalized received signals at both intended and unintended positions. The subsequent focusing gain is presented as a function of the BOF and the number of antennas, enabling us to gain insights in the contributions of each parameter to the system performance. Numerical simulations with multi-path Rayleigh fading channels are carried out to validate the MSE expressions.

© 2020 Elsevier B.V. All rights reserved.

1. Introduction

Time-reversal (TR) is a simple and efficient matched-filter technology for emerging communication systems [1]. It has been shown that with a sufficiently high rate back-off factor (BOF), the TR can create a spatio-temporal focusing effect by collecting the energy from various multipath components [2]. In the literature, the time-domain (TD) implementation of TR precoding has been well investigated [2], while few works focus on the frequency-domain (FD) TR implementation [3]. As mentioned in [2], the focusing effect of TR precoding is achieved when the value of BOF is high. The BOF is defined as the signal up-sampling rate at the transmitter before the precoding process (or the respective

signal down-sampling rate at the receiver before equalization). Thanks to the spatio-temporal focusing gain of TD/TR precoding systems, an equalizer with only one tap is claimed to be generally sufficient in such systems [2], leading to a complexity reduction at the receiver.

Orthogonal frequency-division multiplexing (OFDM) is nowadays a widely-used modulation in new generation wireless systems, as it facilitates the compensation for the frequency selectivity of channel. OFDM modulation has already been used in most of communication systems such as cellular, WiFi, and is also foreseen for underwater [4], optical communications [5]. Moreover, an FD implementation of TR precoding has been shown to be simple and efficient for distributed-antenna multiple-input single-output (MISO) OFDM systems [6,7]. However, previous works have implicitly dealt with BOFs equal to one; thereby, the system does not fully benefit from the focusing effect of TR. Recently, the FD/TR precoding has been investigated with BOFs different from one [3]. However, only the system performance at the intended communication position was considered; hence,

[☆] This document is the research results funded by the Copine-IoT Innoviris project, the Icity.Brussels project and the FEDER/EFRO grant.

* Corresponding author.

E-mail address: trung-hien.nguyen@ulb.ac.be (T.-H. Nguyen).

compared to the other unintended positions, the focusing gain stemming from TR at the intended position was not studied.

In this paper, we investigate the focusing gain (FG) of the FD/TR precoding in MISO OFDM systems when varying the number of antennas and/or BOFs. The focusing gain is defined by the signal-to-noise ratio (SNR) gain, necessary to keep the mean-square-error (MSE) of the received signals unchanged when switching from the intended position to the unintended position. Our main contributions can be summarized as follows:

- We assess for the first time the FG of the FD/TR precoding MISO OFDM system with different number of antennas and BOFs.
- We derive approximated MSE expressions at the intended and unintended positions, and the subsequent FG, for the FD/TR precoding MISO OFDM systems. Similarly to the TD/TR precoding, the MSE of the received symbols at the intended position is shown to be much lower than that at the unintended position, confirming the focusing gain of the FD/TR precoding.
- In order to obtain the MSE approximation at the unintended position, we derive the probability density function (PDF) of the modulus of the sum of products of zero-mean complex Gaussian random variables (RVs) with arbitrary variances. Furthermore, based on the shapes of PDFs of the equivalent channel RVs at the intended and unintended positions, we intuitively show that the diversity and focusing gains at the intended position is bigger than that at the unintended position.
- We analyze the asymptotic behaviors of the MSE expressions to understand in a simple manner the impacts of different used numbers of antennas and BOFs on the MSE when switching from the intended position to the unintended position. Finally, numerical simulations are carried out to validate our analysis.

The remainder of this paper is organized as follows: we present a brief overview of TR in Section 2; the TR-based system model and the proper way to perform TR precoding in the FD are introduced in Section 3; we carry out theoretical performance analyses in Section 4; the asymptotic analysis is conducted in Section 5; we present our analytical and numerical results in Section 6; finally, the paper is concluded in Section 7.

Notation. Column vectors and matrices are presented by lower-case and upper-case bold letters, respectively; the identity matrix of size $N \times N$ and the Fourier matrix of size $Q \times Q$ are denoted by \mathbf{I}_N and \mathbf{F}_Q , respectively; $\Lambda_{\mathbf{x}}$ denotes the diagonal matrix, whose diagonal stacks the elements of the vector \mathbf{x} ; $|\cdot|$, $\|\cdot\|$, $(\cdot)^*$, $(\cdot)^T$, $(\cdot)^H$ are the absolute value, Euclidean norm, complex conjugate, transpose and Hermitian transpose operators, respectively; $\text{tr}\{\cdot\}$ and $\mathbb{E}\{\cdot\}$ are the trace and expectation operators, respectively; the factorial of a positive integer x is presented by $x!$.

2. Time-reversal history

The TR technique was invented to focus the wave energy into one position over the space [8]. Actually, the TR has been first proposed in 1950's in [9], where it was applied to alleviate the delay distortion in a picture transmission system. TR was then investigated in the digital communication in the 1960's, and it has been shown to be the optimal solution of a minimum-transmission-loss constrained optimization problem in the digital communication systems [10].

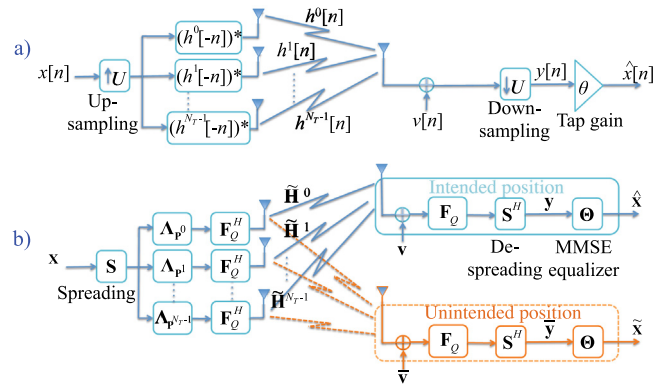


Fig. 1. Schematics of (a) the TD/TR precoding communication system [2] and (b) the corresponding FD/TR precoding OFDM system when communicating with either intended or unintended positions.

TR had been leveraged to improve the performances of the ultrasonic and acoustics systems [8, 11]. Since the nineties, TR has been applied in a lot of applications based on its spatio-temporal focusing effect. For example, the TR imaging technique has been proposed to identify multiple targets within a specific area in combination with the multiple signal classification (MUSIC) algorithm [12]. Target detection using TR-based antenna arrays has been investigated in multipath scattering environments [13]. Recently, TR has been claimed to be a promising candidate for 5G communication systems, where massive multipath (one of the major challenges in modern wireless communications) is exploited to enhance the communication link instead of trying to remove them [14]. TR is also shown to be an interesting technology to provide physical layer security [15], centimeter-accuracy indoor localization [16–18], event detection through a wall [19], and monitoring of vital signs [20]. It is worth noticing that almost all TR-based applications referred here are in the TD. The FD/TR applications, however, did not consider the equivalent TR version as originally invented, i.e., that for which BOF is larger than one.

Due to the fact that OFDM modulation is used widely nowadays – especially in 5G networks, which leverage the use of FD precoding techniques for complexity reduction – the aforementioned TD/TR precoding cannot be easily integrated into modern communication systems. In what follows, we discuss in detail the FD/TR precoding. It is worth noticing that, in the literature, the intended position in some contexts, i.e., secure communications [15], is named as target or legitimate position, while the unintended positions are referred to as the eavesdropper or illegal or non-legitimate positions. In order to make terminologies coherent, we use the “intended position” and “unintended position” terms in this paper. More specifically, we define the “intended position” as the desired position that we want to communicate with. It implies that the channel between the transmitter and the receiver at the desired position is assumed to be perfectly estimated in a first phase [14]. Then the channel is used to time-reversal precode the signal to communicate with the receiver at the desired position in a second phase. In order to assess the focusing gain of time-reversal, we define the “unintended position” as another arbitrary position, so that the precoding vector does not match the channel between the transmitter and that arbitrary position.

3. System model

Fig. 1(a) presents a typical TD/TR precoding MISO system [2]. The time-domain symbol $x[n]$ is U -time (w.r.t. the BOF) up-sampled. Its replicas are sent to N_T transmit antenna branches.

The TR precoding, $(h^k[-n])^*$, with respect to the k th channel impulse response (CIR), $h^k[n]$, are then applied to the signals. After that, the signals are sent to the receiver. After propagating over the channels, an additive white Gaussian noise (AWGN) $v[n]$ is further inserted into the signal. The U -time down-sampled signal can be recovered by a one-tap equalizer with a gain θ . Note that, the minimum mean square error (MMSE) equalizer can be applied to optimize the recovered signal. We assume that the channel information is available in advance at the transmitter and the intended receiver. The channel information can be obtained at the transmitter either by exploiting the channel reciprocity between the uplink and downlink or by implementing a feedback of the channel estimate at the intended receiver to the transmitter. It is well-known in the literature [2] that the focusing gain (FG) is improved in accordance with increasing the BOF and/or the number of antennas. Hence, a better bit-error-rate (BER)/MSE performance can be achieved. However, the signal rate is reduced. Note that, the TR precoding system requires the wideband digital-to-analog converter (DAC) and analog-to-digital converter (ADC) at the transmitter and receiver, respectively. However, we can sample the received signal directly at a low rate, which is equivalent to the rate after the down-sampling by the BOF, thereby simplifying the signal processing.

As aforementioned, the FD/TR precoding system in previous works considered only different numbers of antennas [6,7] with the BOF implicitly equal to one. Recently, a suitable way of TR precoding in the frequency domain has been presented in [3]. We recall here the method to properly map the data onto OFDM symbols (Fig. 1(b)). For the sake of simplicity, only a Q -subcarrier OFDM symbol is transmitted over the FD/TR precoding MISO system. More specifically, we transmit a data vector \mathbf{x} composed of N symbols X_n (for $n = 0, 1, \dots, N-1$ with $N = Q/U$) over the FD/TR precoding system, i.e., $\mathbf{x} = [X_0 \dots X_{N-1}]^T$. Symbols $\{X_n\}$ are complex zero-mean RVs with variance $\mathbb{E}[|X_n|^2] = \sigma_x^2$, which are independent from one to another. Without loss of generality, $\sigma_x^2 = 1$ is considered.

In order to assign the symbols onto the OFDM subcarriers, \mathbf{x} is first multiplied with the $Q \times N$ matrix \mathbf{S} . The matrix \mathbf{S} is formed by concatenating U times $N \times N$ diagonal matrices, which are independent of each other. The diagonal values are chosen randomly from $\{\pm 1\}$ and assumed to be identically and independently distributed (i.i.d.). The matrix \mathbf{S} is scaled by $1/\sqrt{U}$ to obtain $\mathbf{S}^H \mathbf{S} = \mathbf{I}_N$. The design of \mathbf{S} originates from the equivalence between the TD up-sampling of a signal and the FD repetition of its spectrum. Moreover, using a randomized pattern from $\{\pm 1\}$ reduces the similarity among data symbols assigned on various OFDM subcarriers. Hence, a problem of high peak-to-average-power ratio (PAPR) in OFDM systems could be reduced [21].

After mapping data onto OFDM subcarriers, the replicas of the signal are sent to N_T branches associated with transmit antennas. Then, a diagonal matrix $\Lambda_{\mathbf{p}^k}$ w.r.t. the branch k is applied to the signal for precoding. The diagonal elements of matrix $\Lambda_{\mathbf{p}^k}$ are $(H_q^k)^*$ (for $q = 0, 1, \dots, Q-1$), where H_q^k is the q th component of the channel frequency response (CFR) \mathbf{h}^k corresponding to the antenna k . We define $\mathbf{h}^k \triangleq [H_0^k H_1^k \dots H_{Q-1}^k]^T$ and assume a normalized total channel power. After that, an inverse fast Fourier transformation (IFFT) is applied to FD/TR precoded signals to convert the signal to the TD. A cyclic prefix (CP) is inserted into (resp. removed out of) the signal at the transmitter (resp. at the receiver). The propagation of the signal over the channel is mathematically represented as the signal multiplication with the circulant matrix $\tilde{\mathbf{H}}^k$ of size $Q \times Q$ (w.r.t. the k -th CIR). Thanks to the CP insertion/removal, $\tilde{\mathbf{H}}^k$ is decomposed as $\tilde{\mathbf{H}}^k = \mathbf{F}_Q^H \cdot \Lambda_{\mathbf{h}^k} \cdot \mathbf{F}_Q$, where the diagonal matrix $\Lambda_{\mathbf{h}^k}$ contains the elements

of vector \mathbf{h}^k on its diagonal. It is worth noticing that $\Lambda_{\mathbf{h}^k}$ is associated to an arbitrary position, which may or may not be the intended position, i.e., that for which the precoding matrix $\Lambda_{\mathbf{p}^k}$ is computed. The reversed operations are made at the receiver side in order to recover the signal. It should be noted that the TR precoding system requires a wideband ADC. However, the receiver can work directly at a low-rate that is equal to the symbol rate after de-mapping operation. It is implicitly considered that the front-end oscillators up-convert (resp. down-convert) the signal to the band-pass (resp. baseband) signal. Therefore, the symbols are assigned onto OFDM subcarriers without using the Hermitian symmetry property. We also consider the perfect synchronization, the received signal at the intended position can be given by

$$\mathbf{y} = \mathbf{S}^H \cdot \mathbf{F}_Q \cdot \left(\sum_{k=0}^{N_T-1} \tilde{\mathbf{H}}^k \cdot \mathbf{F}_Q^H \cdot \Lambda_{\mathbf{p}^k} \right) \cdot \mathbf{S} \cdot \mathbf{x} + \mathbf{v}', \quad (1)$$

where $\mathbf{v}' = \mathbf{S}^H \mathbf{F}_Q \mathbf{v} \triangleq [V'_0 \dots V'_{N-1}]^T$ represents the FD version of the TD AWGN \mathbf{v} with the variance $\sigma_{v'}^2$. The RVs X_n and V'_n are assumed to be independent from one to another. The autocorrelation matrix of the noise is defined as $\mathbf{R}_{\mathbf{v}\mathbf{v}'} \triangleq \mathbb{E}[\mathbf{v} \cdot \mathbf{v}'^H] = \sigma_{v'}^2 \mathbf{I}_Q$. From the definition of the matrix \mathbf{S} , we can easily obtain $\mathbf{R}_{\mathbf{v}\mathbf{v}'} = \sigma_{v'}^2 \mathbf{I}_N$. We can now rewrite (1) as $\mathbf{y} = \mathbf{G} \cdot \mathbf{x} + \mathbf{v}'$, in which $\mathbf{G} = \mathbf{S}^H \cdot \left(\sum_{k=0}^{N_T-1} \Lambda_{\mathbf{h}^k} \cdot \Lambda_{\mathbf{p}^k} \right) \cdot \mathbf{S}$.

In this paper, a MMSE equalization with one tap is used to equalize the received signal after de-mapping by matrix \mathbf{S}^H . The MMSE equalizer is represented by $\Theta = (\mathbf{G}^H \cdot \mathbf{G} + \gamma^{-1} \mathbf{I}_N)^{-1} \cdot \mathbf{G}^H$ (where the SNR γ is defined as $\gamma \triangleq \sigma_x^2 / \sigma_{v'}^2$). The estimate $\hat{\mathbf{x}}$ of the input signal vector is then deduced by $\hat{\mathbf{x}} = \Theta \cdot \mathbf{y}$. It is worth noticing that at the intended position, Θ becomes a real-valued diagonal matrix, because the channel matches the TR precoding, resulting in a reduction of the receiver complexity. At the unintended position, the same mathematical model can be built similarly. In order to make a fair performance comparison between intended and unintended positions, we assume that the same variance of AWGNs is used at both positions. Furthermore, the MMSE equalizer is also applied at the unintended position with the knowledge of the equivalent channel. Note that, the TR precoding is not matched to the channels at the unintended position, consequently Θ is now a complex-valued diagonal matrix, thereby requiring more receiver complexity. It is also worth noting that compared to TD/TR precoding, the FD/TR precoding system provides two major advantages: (1) it is easy to integrate the precoder into the existing OFDM transmitter (subcarrier-multiplication-wise versus convolution); (2) a real-valued equalizer can be applied at a low rate at the receiver.

4. Performance assessment

We define the error of estimated symbol as $\mathbf{e} \triangleq \mathbf{x} - \hat{\mathbf{x}}$ and the error-autocorrelation matrix as $\mathbf{R}_{\mathbf{e}\mathbf{e}} \triangleq \mathbb{E}[\mathbf{e} \cdot \mathbf{e}^H]$. The performance of FD/TR precoding system is assessed based on the MSE of the equalized received symbol, and it is derived as follows¹

$$MSE = \text{tr}\{\mathbf{R}_{\mathbf{e}\mathbf{e}}\} = \sigma_{v'}^2 \text{tr} \left\{ \mathbb{E} \left[\left(\mathbf{G}^H \cdot \mathbf{G} + \gamma^{-1} \mathbf{I}_N \right)^{-1} \right] \right\}. \quad (2)$$

In order to assess the focusing gain (FG) of TR, we compare the normalized MSEs (NMSEs) (defined as $NMSE \triangleq MSE / (N\sigma_x^2)$) of the received signal at both the intended and unintended communication positions. Due to the fact that \mathbf{G} is a diagonal matrix,

¹ Note that, all the expectations from now on are implicitly carried out over the signal, noise and channel RVs.

the NMSE is given by

$$NMSE = \frac{1}{N} \sum_{n=0}^{N-1} \mathbb{E} \left[\frac{\gamma^{-1}}{\frac{1}{U^2} |K_n|^2 + \gamma^{-1}} \right], \quad (3)$$

where K_n is a random variable (RV) depending on the communication position. More particularly, at the intended position, $K_n = \sum_{k=0}^{N_T-1} \sum_{u=0}^{U-1} |H_{n+uN}^k|^2$ and at the unintended position, $K_n = \sum_{k=0}^{N_T-1} \sum_{u=0}^{U-1} \bar{H}_{n+uN}^k \cdot (H_{n+uN}^k)^*$, in which \bar{H}_n^k is the n th component of the unintended position CFR associated with the k th transmit antenna. We assume that the channels at the intended and unintended positions are spatially independent.

We further consider the L -tap CIRs between each transmit antenna and the receive antenna. The CIR taps are assumed to be independent (equivalent to taps constructed by uncorrelated scattering). The variance of the l th CIR tap is $\sigma_{h_l}^2 = \mathbb{E}[|h_l|^2]$. We also consider a Rayleigh fading channel. Thanks to the design of the matrix \mathbf{S} as described in Section 3, the RV K_n in (3) is constructed by the sum of weakly correlated complex RVs. When the BOF value is small or moderate, RVs H_{n+uN}^k and $H_{n+(u+1)N}^k$ (for $\forall n \in [0, N-1]$, $\forall k \in [0, N_T-1]$ and $\forall u \in [0, U-2]$) can be considered to be independent from one to another and identically distributed so that the NMSE in (3) can be approximated by

$$NMSE \approx \mathbb{E} \left[\frac{\gamma^{-1}}{\frac{1}{U^2} |K_n|^2 + \gamma^{-1}} \right]. \quad (4)$$

- At the intended position:

Although the NMSE has been derived in [3], we reproduce it here to facilitate the evaluation of the FG. Furthermore, more series expansion terms, i.e., second and third orders of the Taylor series expansion (detailed in Appendix A), are used here to improve the approximation. The RV K_n has the PDF $f_Z(z) = z^{M-1} e^{-z} / (M-1)!$ [22], where $M = UN_T$. Applying this PDF to (4), we obtain a closed-form NMSE expression

$$NMSE \approx \frac{\gamma^{-1}}{(M-1)!} \int_0^\infty \frac{z^{M-1}}{z^2/U^2 + \gamma^{-1}} e^{-z} dz. \quad (5)$$

Although (5) can be numerically computed, it is still difficult to analyze the asymptotic behaviors. We therefore approximate (5) as in Appendix A to yield a tractable NMSE approximation at the intended position, $f_{int}(\gamma, U, N_T)$, as follows

$$\begin{aligned} f_{int}(\gamma, U, N_T) &\approx \frac{1}{(UN_T - 1)!} (\Gamma_{low}(UN_T, U\gamma^{-1/2}) \\ &\quad - \frac{1}{U^2\gamma^{-1}} \Gamma_{low}(UN_T + 2, U\gamma^{-1/2}) \\ &\quad + \frac{1}{U^4\gamma^{-2}} \Gamma_{low}(UN_T + 4, U\gamma^{-1/2}) \\ &\quad + U^2\gamma^{-1} \Gamma_{up}(UN_T - 2, U\gamma^{-1/2}) \\ &\quad - U^4\gamma^{-2} \Gamma_{up}(UN_T - 4, U\gamma^{-1/2})). \end{aligned} \quad (6)$$

in which Γ_{low} and Γ_{up} are the lower and upper incomplete Gamma functions, respectively, and defined by

$$\Gamma_{low}(a, t) = \int_0^t x^{a-1} e^{-x} dx, \quad (7)$$

and

$$\Gamma_{up}(a, t) = \int_t^\infty x^{a-1} e^{-x} dx, \quad (8)$$

such that $\Gamma_{low}(a, t) + \Gamma_{up}(a, t) = \Gamma(a)$ is the Gamma function.

Table 1

PDP of the Extended Pedestrian A (EPA) channel.

| Excess tap delay (ns) | Relative power (dB) |
|-----------------------|---------------------|
| 0 | 0.0 |
| 30 | -1.0 |
| 70 | -2.0 |
| 90 | -3.0 |
| 110 | -8.0 |
| 190 | -17.2 |
| 410 | -20.8 |

-At the unintended position:

In order to derive a closed-form NMSE approximation, we have to know the PDF of the RV $|K_n|$. This PDF is derived in the following theorem.

Theorem 1. Let a RV $Z_m = Y_{1,m} \cdot Y_{2,m}$, where $Y_{1,m}$ and $Y_{2,m}$ are statistically independent and identically distributed (i.i.d) complex Gaussian RVs of zero-mean and variance $\sigma_{Y_1}^2$ and $\sigma_{Y_2}^2$, respectively, i.e., $Y_{1,m} \sim \mathcal{CN}(0, \sigma_{Y_1}^2)$, $Y_{2,m} \sim \mathcal{CN}(0, \sigma_{Y_2}^2)$. Considering $Z = \sum_{m=0}^{M-1} Z_m$, then the modulus of Z , $R = |Z|$, has the following PDF

$$f_R(r) = \frac{4r^M}{\Gamma(M) \cdot (\sigma_{Y_1}\sigma_{Y_2})^{M+1}} \mathbb{K}_{M-1} \left(\frac{2r}{\sigma_{Y_1}\sigma_{Y_2}} \right), \quad (9)$$

where $\mathbb{K}_M(\cdot)$ is the M th order modified Bessel function of the second kind.

Proof. See Appendix B.

In our study, we consider a normalized total channel power, which also induces that the variances of RVs H_n^k and \bar{H}_n^k are equal to one. Substituting the result of the theorem into (4), we obtain the following closed-form NMSE expression at the unintended position

$$NMSE \approx \frac{4\gamma^{-1}}{\Gamma(M)} \int_0^\infty \frac{z^M}{z^2/U^2 + \gamma^{-1}} \mathbb{K}_{M-1}(2z) dz. \quad (10)$$

In order to get a tractable NMSE expression to further evaluate the asymptotic behaviors, we apply the series expansion of the modified Bessel function of the second kind [23, eq. (24)]

$$\mathbb{K}_M(x) \approx \sum_{q=0}^D \sum_{l=q}^D \Psi(M, l, q) \cdot e^{-x} \cdot x^{q-M}, \quad (11)$$

where D specifies the number of expansion terms, $\Psi(M, l, q)$ is a coefficient given by

$$\Psi(M, l, q) = \frac{(-1)^q \sqrt{\pi} \cdot \Gamma(2M) \cdot \Gamma(\frac{1}{2} + l - M) \cdot \mathbb{L}(l, q)}{2^{M-q} \cdot \Gamma(\frac{1}{2} - M) \cdot \Gamma(\frac{1}{2} + l + M) \cdot l!} \quad (12)$$

and $\mathbb{L}(l, q) = \binom{l-1}{q-1} \frac{l!}{q!}$ for $\forall l, q > 0$ is the Lah number [23] with the conventions $\mathbb{L}(0, 0) = 1$, $\mathbb{L}(l, 0) = 0$, $\mathbb{L}(l, 1) = l!$ for $\forall l > 0$.

Since the order $M-1$ of the modified Bessel function of the second kind in (10) is a non-negative integer number, the series representation (11) converges except for $M-1=0$ [23]. However, $\mathbb{K}_0(x)$ can be computed from the series representations of $\mathbb{K}_1(x)$ and $\mathbb{K}_2(x)$ based on the recurrence identity: $\mathbb{K}_0(x) = \mathbb{K}_2(x) - 2x^{-1}\mathbb{K}_1(x)$ [24].

Based on the derivation in Appendix C, the tractable closed-form NMSE approximation, $f_{unint}(\gamma, U, N_T)$, can be obtained

$$f_{unint}(\gamma, U, N_T)$$

$$\approx \left\{ \begin{array}{l} \frac{1}{(UN_T - 1)!} \sum_{q=0}^D \mathbb{G}_{UN_T}(q) \left[\frac{1}{2^{UN_T-1}} \Gamma_{low}(q+2, 2U\gamma^{-1/2}) \right. \\ \quad - \frac{1}{2^{UN_T+1}U^2\gamma^{-1}} \Gamma_{low}(q+4, 2U\gamma^{-1/2}) \\ \quad + \frac{1}{2^{UN_T+3}U^4\gamma^{-2}} \Gamma_{low}(q+6, 2U\gamma^{-1/2}) \\ \quad + \frac{U^2\gamma^{-1}}{2^{UN_T-3}} \Gamma_{up}(q, 2U\gamma^{-1/2}) \\ \quad \left. - \frac{U^4\gamma^{-2}}{2^{UN_T-5}} \Gamma_{up}(q-2, 2U\gamma^{-1/2}) \right], \\ \quad \text{if } UN_T > 1 \\ \\ \sum_{q=0}^D \mathbb{G}_1(q) \left[\Gamma_{low}(q, 2U\gamma^{-1/2}) \right. \\ \quad - \frac{1}{4 \cdot U^2\gamma^{-1}} \Gamma_{low}(q+2, 2U\gamma^{-1/2}) \\ \quad + \frac{1}{16 \cdot U^4\gamma^{-2}} \Gamma_{low}(q+4, 2U\gamma^{-1/2}) \\ \quad + 4 \cdot U^2\gamma^{-1} \Gamma_{up}(q-2, 2U\gamma^{-1/2}) \\ \quad \left. - 16 \cdot U^4\gamma^{-2} \Gamma_{up}(q-4, 2U\gamma^{-1/2}) \right], \\ \quad \text{if } UN_T = 1 \end{array} \right. \quad (13)$$

in which $\mathbb{G}_{UN_T}(q)$ is calculated as follows

$$\left\{ \begin{array}{l} \mathbb{G}_{UN_T}(q) = \sum_{l=q}^D \Psi(UN_T - 1, l, q), \quad \text{if } UN_T > 1 \\ \\ \mathbb{G}_1(q) = \sum_{l=q}^D (\Psi(2, l, q) - 2 \cdot \Psi(1, l, q)), \quad \text{if } UN_T = 1 \end{array} \right. \quad (14)$$

The FG at a certain NMSE can finally be deduced by

$$FG = \gamma_{unint} - \gamma_{int} \quad (15)$$

s.t. $f_{int}(\gamma_{int}, U, N_T) = f_{unint}(\gamma_{unint}, U, N_T)$

As the direct inversion problem to compute the SNR associated with a predefined NMSE at both the intended (f_{int}) and unintended (f_{unint}) positions is non-trivial, we first compute the NMSE as a function of the SNR with an arbitrary SNR step, i.e., 0.1 dB. Then we deduce the SNR with respect to the predefined NMSE. The accuracy of this SNR computation can easily be improved by either interpolation or reduction of SNR step.

5. Asymptotic analysis

We derive here the asymptotic (in SNRs, BOFs U and the number of antennas N_T parameters) behaviors of the NMSE approximations to gain insights.

- *At the intended position:*

Considering (6) at high SNR, due to the fact that $U\gamma^{-1/2} \approx 0$, as a consequence $\Gamma_{low}(s, U\gamma^{-1/2}) \approx 0$ and $\Gamma_{up}(s, U\gamma^{-1/2}) \approx \Gamma(s)$. In (6), the value of the fourth term is much bigger than that of the fifth term. The NMSE at high SNR, $f_{int}^{high}(\gamma, U, N_T)$, is approximated by

$$f_{int}^{high}(\gamma, U, N_T) \approx \frac{U^2\gamma^{-1}\Gamma(UN_T - 2)}{(UN_T - 1)!} \quad (16)$$

Taking into account the fact that $\Gamma(a) = (a - 1)!$ if a is a positive integer, and considering $UN_T > 2$, (16) is reduced to

$$f_{int}^{high}(\gamma, U, N_T) \approx \frac{\gamma^{-1}}{(N_T - 1/U)(N_T - 2/U)} \xrightarrow{U \rightarrow +\infty} \frac{\gamma^{-1}}{(N_T)^2} \quad (17)$$

Inspecting (17) reveals that if a sufficiently high BOF is applied, the NMSE is only improved by using more antennas. It is confirmed later in the simulation results.

Considering (6) at low SNR, the proposed NMSE approximation $f_{int}^{low}(\gamma, U, N_T)$ is

$$f_{int}^{low}(\gamma, U, N_T) \approx \frac{\Gamma_{low}(UN_T, U\gamma^{-1/2})}{(UN_T - 1)!} \quad (18)$$

because in (6) the second and third terms are smaller than the first term, whereas the fourth and fifth terms are approximately equal to 0. Applying the series expansion $\Gamma_{low}(a, t) = t^a \Gamma(a) e^{-t} \sum_{k=0}^{\infty} t^k / \Gamma(a + k + 1)$ [25, eqs. (8.2.6) and (8.7.1)], we can easily achieve the approximated NMSE as follows

$$f_{int}^{low}(\gamma, U, N_T) \approx 1 - e^{-U\gamma^{-1/2}} \sum_{k=1}^{UN_T} \frac{(U\gamma^{-1/2})^{UN_T-k}}{(UN_T - k)!} \quad (19)$$

Inspecting (19) reveals that a similar conclusion as for $f_{int}^{high}(\gamma, U, N_T)$ can be made for $f_{int}^{low}(\gamma, U, N_T)$. More particularly, when the BOF U is big enough, increasing the number of antennas N_T is the only way to improve $f_{int}^{low}(\gamma, U, N_T)$. As considering a fixed value of N_T , increasing U makes the reduction of the term $e^{-U\gamma^{-1/2}}$ much quicker than the summation term of (19), leading to an un-changed $f_{int}^{low}(\gamma, U, N_T)$ value. If we set U to a specific value, by increasing N_T , we can reduce the value of $f_{int}^{low}(\gamma, U, N_T)$ since the summation has more terms.

- *At the unintended position:*

At high SNR, similar to the analysis at the intended position, only the terms with $\Gamma_{up}(\cdot)$ have a significant contribution to the NMSE. Considering $UN_T > 1$ for the sake of simplicity, (13) can be approximated to

$$f_{unint}^{high}(\gamma, U, N_T) \approx \frac{\gamma^{-1}\sqrt{\pi}U^2 \cdot \Gamma(2(UN_T - 1))}{2^{2UN_T-4} \cdot \Gamma(UN_T)} \times \sum_{q=0}^D \sum_{l=q}^D \frac{(-2)^q \Gamma(\frac{3}{2} - UN_T + l) \mathbb{L}(l, q) \Gamma_{up}(q, 2U\gamma^{-1/2})}{\Gamma(\frac{3}{2} - UN_T) \Gamma(UN_T - \frac{1}{2} + q) q!} \quad (20)$$

By virtue of $\Gamma(UN_T) = (UN_T - 1) \Gamma(UN_T - 1)$ and applying the Legendre duplication formula to $\Gamma(2(UN_T - 1))$, (20) is rewritten as

$$f_{unint}^{high}(\gamma, U, N_T) \approx 2\gamma^{-1} \frac{U^2}{(UN_T - 1)} \times \sum_{q=1}^D \sum_{l=q}^D \frac{(-2)^q \mathbb{L}(l, q) \Gamma(q) \Gamma(UN_T - \frac{1}{2}) \Gamma(\frac{3}{2} - UN_T + l)}{q! \Gamma(\frac{3}{2} - UN_T) \Gamma(UN_T - \frac{1}{2} + q)} \quad (21)$$

It can be observed that both numerator and denominator of the fraction term inside the summation of (21) are proportional to $U^2 N_T^2$, therefore this fraction asymptotically converges to a constant when increasing UN_T . Considering U and N_T as the variables, $f_{unint}^{high}(\gamma, U, N_T)$ is proportional to the following expression

$$f_{unint}^{high}(\gamma, U, N_T) \propto \frac{U^2}{UN_T - 1} \quad (22)$$

It can be concluded from (22) that increasing the BOF U causes the increase of NMSE (or equivalently decreases the focusing gain). The NMSE can be reduced by using more transmit antennas.

The same analysis and conclusion can be drawn for low SNRs, we skip it as it does not bring any additional insight.

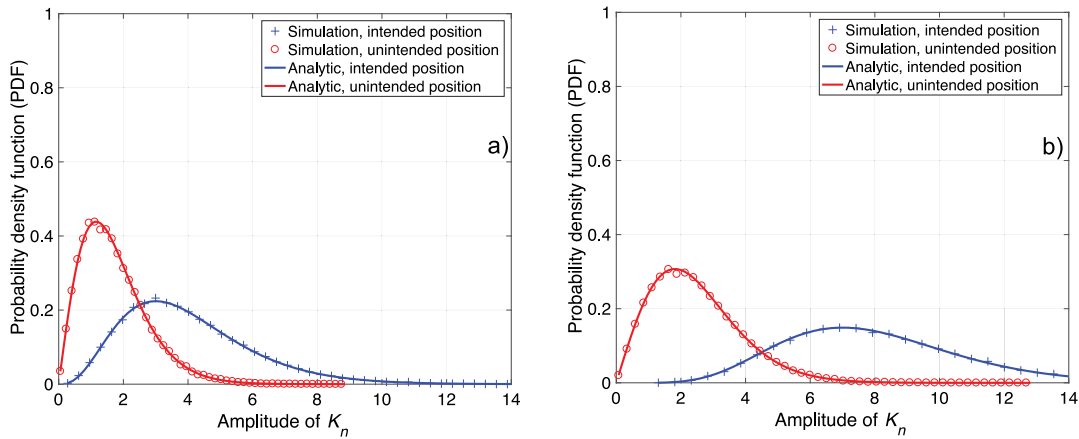


Fig. 2. Probability density function (PDF) envelopes of the RV K_n at the intended and unintended positions. (a) $M = 4$; (b) $M = 8$.

6. Simulation results

A FD/TR precoding MISO OFDM system is considered. We set the number of OFDM subcarriers to 256, i.e., $Q = 256$. A multi-path Rayleigh fading channel of type Extended Pedestrian A (EPA) [26] is used in the simulations. Its power delay profile (PDP) is given in Table 1 and normalized to unity for the fair performance comparison between intended and unintended positions. We assume that the channel is perfectly known at the transmitter. The impact of imperfect channel estimation on the TR-based system performance has been studied in [27] (and references therein), but is beyond the scope of this paper. Note that, we set the number of the expansion term of modified Bessel function $D = 20$ in the following computations. The analytical results at the intended and unintended positions are presented by the solid-lines and dashed-lines, respectively. The numerical results with respect to either intended or unintended positions are plotted with marker symbols.

As the RV K_n in (4) can intuitively be related to the diversity gain given by the TR focusing and the use of multiple antennas, we consider the distribution of K_n at the intended and unintended positions in Fig. 2 when $M = 4$ and $M = 8$ based on derived PDFs. It can be seen that the analytical PDFs match the numerical ones.² At the intended position, the TR precoding matches the channel, while there is a mismatch between the precoding and channel at the unintended position. Consequently, the values of RV K_n at the intended position are distributed in a wider range than that at the unintended position (i.e., when $M = 4$, the value of K_n is mainly distributed from 0.2 up to 11 at the intended position, while it falls between 0.1 and 5 at the unintended position). When increasing M from 4 to 8, the distribution of K_n value increases accordingly. The bigger value of K_n can get, the more diversity gain can achieve. In other words, the bigger value of K_n in (4) leads to a smaller NMSE value. It implicitly explains that the NMSE at the intended position is smaller than that at the unintended position when increasing M .

In the first step, we evaluate the NMSE as a function of the SNR at the intended position in Fig. 3. Fig. 3(a) shows NMSE evolution for different number of antennas, when U is equal to 2. Fig. 3(b) presents NMSE evolution for different BOFs, when N_T is set to 2. As expected, the analytical closed-form NMSEs match the ones obtained by simulations, confirming the correctness of our derivation in (6). The simulation results also confirm our previous observation that when increasing the BOF, the NMSE

(and hence the spatio-temporal focusing) converges asymptotically to an NMSE lower bound (presented in (17)). It is observed that increasing the number of antennas continuously provides the focusing gain. For instance, in order to obtain a $\text{NMSE} = -20$ dB, by changing the number of antennas from one to two, we achieve a SNR gain of about 12 dB, while by using a BOF of two instead of one, we can only obtain a SNR gain of about 6 dB.

We now evaluate the NMSE as a function of the SNR at the unintended position in Fig. 4 with different number of antennas when U is equal to 2 (Fig. 4(a)) and with different BOFs when N_T is set to 2 (Fig. 4(b)). Similar to the results at the intended position, the numerical NMSEs follow the predicted analytical ones in (13). The simulation results also confirm the asymptotic analyses that the NMSE can only improve by increasing the number of antennas, while, in contrast to the case at the intended position, increasing the BOF gives a poorer MSE. For instance, at NMSE equal to -20 dB, by changing the number of antennas from one to two, we achieve about 4 dB SNR gain (much less than that at the intended position), while by using a BOF of two instead of one, the SNR loss is about 0.6 dB. In the case that $N_T = 1$ and $U = 2$, the system at the intended position (where the precoder matches the channel) benefits from the frequency-diversity gain, even if there is no spatial-diversity gain. It explains why the NMSE value at the unintended position is larger than that at the intended position.

The MSEs at the intended and unintended positions are compared in Fig. 5. It can be observed that when changing from the no-focusing-gain case ($U = N_T = 1$) to the case where $U = N_T = 4$ and considering the $\text{NMSE} = -20$ dB, the SNR gain at the intended position is about 22 dB bigger than that at the unintended position, confirming again the focusing effect provided by the TR precoding. It is also reminded that the SNR gain at the unintended position is provided by only the increase of the number of antennas. Surprisingly, we observe from the no-focusing-gain case that the NMSE value at the unintended position is smaller than that at the intended position for the moderate and high SNRs (Fig. 5). Rigorously, we can explain this fact based on the Eqs. (6) and (13) by considering their monotonicities in the interesting SNR range. Intuitively, it can be explained because the precoded channels at the unintended position are complex, while the precoded channels at the intended position are real, resulting in a less deep fading probability at the subcarrier-level of the equivalent channel magnitude.

Finally, we investigate the focusing gain when varying the number of antennas and BOFs and the targeted NMSE is fixed to -10 dB. The results are presented in Fig. 6. The numerical results confirm again the observation made in the analyses that by increasing either the number of antennas or BOFs, we can improve

² Due to the normalized channel generation, the variance of K_n is equal to one. Other values of variances of K_n are also verified but not shown here.

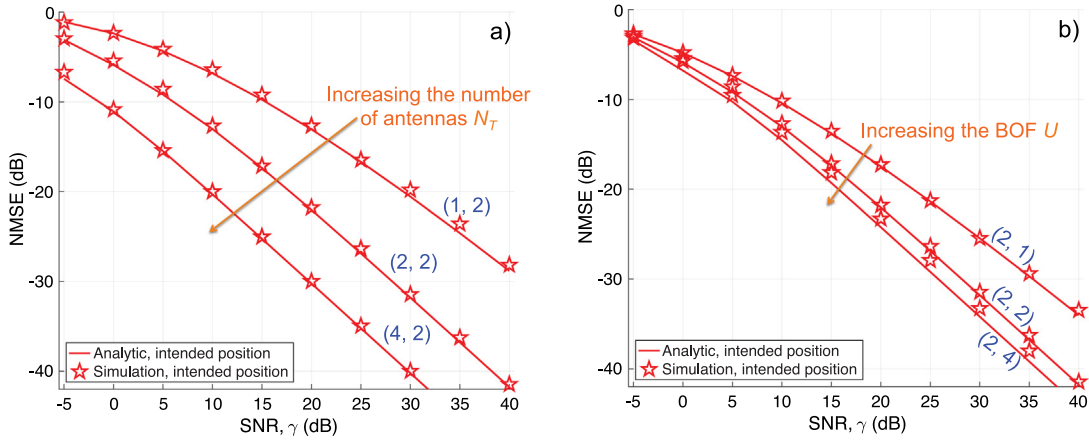


Fig. 3. NMSE versus SNR at the intended position. (a) Different number of antennas when $U = 2$, (b) Different BOFs when $N_T = 2$. The couple (N_T, U) is indicated on each curve.

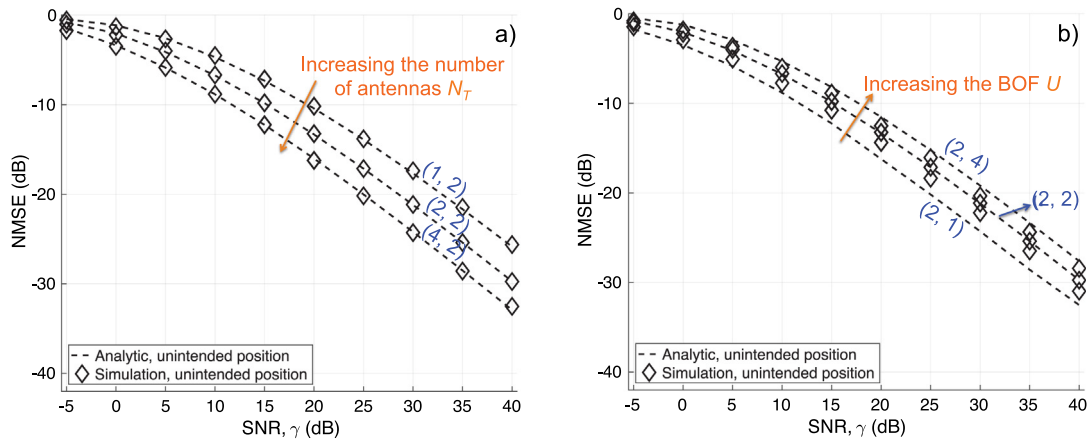


Fig. 4. NMSE versus SNR at the unintended position. (a) Different number of antennas when $BOF = 2$, (b) Different BOFs when $N_T = 2$. The couple (N_T, U) is indicated on each curve.

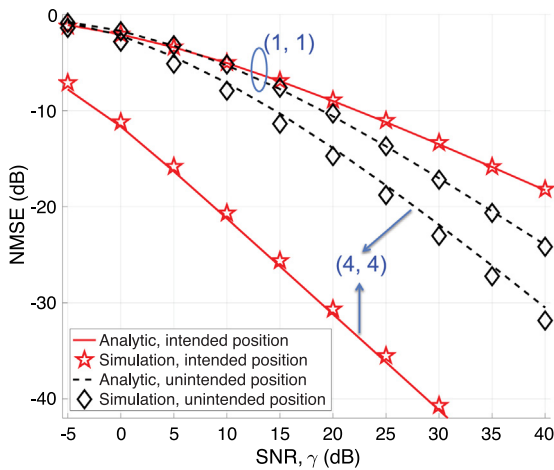


Fig. 5. NMSE versus SNR at both intended and unintended positions when increasing the number of antennas and BOFs. The couple (N_T, U) is indicated on each curve.

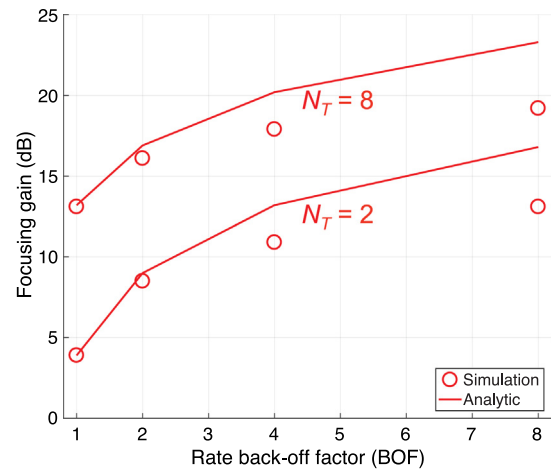


Fig. 6. Focusing gain at the targeted NMSE of -10 dB as a function of the rate back-off factor when the number of antennas are equal to 2 and 8.

the focusing gain. It is worth reminding that the focusing gain is defined by the SNR gain necessary to keep the MSE at a fixed value. At the intended position, the RV K_n is built constructively thanks to the TR precoding of the signal with the corresponding CFR. This leads to the reduction of the NMSE and hence improves

the focusing gain, especially when increasing BOFs (associated with the frequency diversity gain). On the contrary, at the unintended position, the RV K_n is constructed destructively from $(H_n^k)^*$ and \bar{H}_n^k associated with the CFR component at the unintended position, because of their spatial independence. This causes the

increase in the NMSE in (3) when increasing the BOFs. In the case we increase the number of antennas, the NMSEs in both intended and unintended positions are reduced thanks to the spatial diversity gain. However, the SNR gain at the unintended position is smaller than that at the intended position, since the spatial diversity gain at the unintended position can partially compensate for the destructive construction of the RV K_n (originating from the BOF). It should also be noted that when the BOF value is high, the assumption of the statistical independence among RVs H_n does not hold so that there are some mismatches between the analytical and numerical results. Based on [28, Theorem 2], when $N_T \rightarrow \infty$, the NMSE reduces unboundedly. As a consequence, from Eqs. (17) and (22), γ_{int} and γ_{unint} (constrained by predefined NMSE, i.e., Eq. (15)) are proportional to different orders of N_T , the FG hence increases unboundedly when $N_T \rightarrow \infty$. Without loss of generality, we further assume that $N_T \geq U$. Based on this assumption, it can be shown that γ_{int} and γ_{unint} converge asymptotically to specific values, when $U \rightarrow \infty$. It means that the FG converges asymptotically, when $U \rightarrow \infty$. Intuitively, due to the limited OFDM symbol length, the frequency-diversity gain cannot be exploited anymore when increasing the BOF.

In terms of complexity, we assess the number of multiplications necessary to implement the communication with the intended position. Based on Fig. 1(b), the multiplications appear in (1) Spreading (de-spreading); (2) Precoding; (3) FFT (IFFT) operators; and (4) equalization. Note that, the product of two complex numbers requires 4 real-valued multiplications, denoted as \otimes . More specifically:

- The spreading (and de-spreading) process requires $4N \cdot U \otimes$.
- The precoding operation requires $4N \cdot U \cdot N_T \otimes$.
- Knowing that an FFT/IFFT of size $N \cdot U$ requires $N \cdot U(\log_2(N \cdot U) - 3) + 4 \otimes$ using the split-radix algorithm [29], the overall FFT (IFFT) operators need $(N_T + 1) \cdot N \cdot U(\log_2(N \cdot U) - 3) + 4 \otimes$.
- Assuming that the real-valued equalizer coefficients are computed in advance, the equalizer requires only $2N \otimes$.

In total, the complexity in terms of real-valued multiplications is $(N_T + 1) \cdot N \cdot U(\log_2(N \cdot U) + 1) + 2N + 4$. The complexity hence increases when using the high number of antennas N_T and/or BOFs U .

7. Conclusion

We have investigated the FD/TR precoding in the MISO OFDM communication system with BOFs different to one, when communicating to either intended or unintended positions. We have also verified the focusing gain (provided by the FD/TR precoding), which is defined as the SNR gain required to maintain a fixed value of MSE. By evaluating the normalized MSE (NMSE), it is shown that, at the intended position, using a high number of antennas and/or BOFs improves the focusing gain. Conversely, at the unintended position, the useful received power is lower. The approximated NMSE expressions at the intended and unintended positions and the subsequent focusing gain have been derived and validated through simulations.

CRedit authorship contribution statement

Trung-Hien Nguyen: Presented the basic idea, Derived the NMSE and focusing gain expressions, Writing - original draft, Prepared the numerical and analytical results, Contributed to the developing the research ideas, Involved in the discussion of results, Writing - review & editing. **Jean-François Determe:** Prepared the numerical and analytical results, Writing - review & editing. **Shaghayegh Monfared:** Prepared the numerical and analytical results, Writing - review & editing. **Jérôme Louveaux:**

Contributed to the developing the research ideas, Involved in the discussion of results, Writing - review & editing. **Philippe De Doncker:** Contributed to the developing the research ideas, Involved in the discussion of results, Writing - review & editing. **François Horlin:** Presented the basic idea, Derived the NMSE and focusing gain expressions, Writing - original draft, Contributed to the developing the research ideas, Involved in the discussion of results, Writing - review & editing.

Declaration of competing interest

The authors declare that they have no known competing financial interests or personal relationships that could have appeared to influence the work reported in this paper.

Appendix A. Appendix I

At the intended position, based on the PDF of K_n , (5) can be rewritten as

$$\begin{aligned} \text{NMSE} &\approx \int_0^\infty \frac{\gamma^{-1}}{z^2/U^2 + \gamma^{-1}} \frac{z^{M-1}}{(M-1)!} e^{-z} dz \\ &\approx \frac{1}{(M-1)!} \left(\int_0^{U\gamma^{-1/2}} \frac{\gamma^{-1}}{z^2/U^2 + \gamma^{-1}} z^{M-1} e^{-z} dz \right. \\ &\quad \left. + \int_{U\gamma^{-1/2}}^\infty \frac{\gamma^{-1}}{z^2/U^2 + \gamma^{-1}} z^{M-1} e^{-z} dz \right). \end{aligned} \quad (23)$$

In order to ensure the convergence of the integral, we split the NMSE integral into two parts with two ranges of interest $T_1 = \int_0^{U\gamma^{-1/2}} \frac{\gamma^{-1} z^{M-1} e^{-z}}{z^2/U^2 + \gamma^{-1}} dz$ and $T_2 = \int_{U\gamma^{-1/2}}^\infty \frac{\gamma^{-1} z^{M-1} e^{-z}}{z^2/U^2 + \gamma^{-1}} dz$. Then T_1 can be derived as

$$\begin{aligned} T_1 &= \int_0^{U\gamma^{-1/2}} \left(1 + \frac{z^2}{U^2\gamma^{-1}} \right)^{-1} z^{M-1} e^{-z} dz \\ &\approx \int_0^{U\gamma^{-1/2}} \left(1 - \frac{z^2}{U^2\gamma^{-1}} + \frac{z^4}{U^4\gamma^{-2}} \right) z^{M-1} e^{-z} dz, \end{aligned} \quad (24)$$

where the approximation is based on the Taylor expansion $(1+x)^{-1} = \sum_{n=0}^\infty (-x)^n$, whose convergence is guaranteed on the range of the integral $(0, U\gamma^{-1/2})$, as $z^2/(U^2\gamma^{-1}) < 1$. Applying the lower incomplete Gamma function defined in (7) into (24), we achieve the approximated formula of T_1

$$\begin{aligned} T_1 &\approx \Gamma_{\text{low}}(M, U\gamma^{-1/2}) - \frac{1}{U^2\gamma^{-1}} \Gamma_{\text{low}}(M+2, U\gamma^{-1/2}) \\ &\quad + \frac{1}{U^4\gamma^{-2}} \Gamma_{\text{low}}(M+4, U\gamma^{-1/2}). \end{aligned} \quad (25)$$

Because $U^2\gamma^{-1}/z^2 < 1$, T_2 can be derived in the similar way by applying the Taylor expansion, as the convergence on the range of the integral $(U\gamma^{-1/2}, \infty)$ is ensured, we first rewrite T_2 as follows

$$\begin{aligned} T_2 &= \int_{U\gamma^{-1/2}}^\infty U^2\gamma^{-1} z^{-2} \left(1 + \frac{U^2\gamma^{-1}}{z^2} \right)^{-1} z^{M-1} e^{-z} dz \\ &\approx \int_{U\gamma^{-1/2}}^\infty U^2\gamma^{-1} z^{-2} \left(1 - \frac{U^2\gamma^{-1}}{z^2} \right) z^{M-1} e^{-z} dz. \end{aligned} \quad (26)$$

Substituting the upper incomplete Gamma function defined in (8) into (26), the approximated formula of T_2 is

$$T_2 \approx U^2\gamma^{-1} \Gamma_{\text{up}}(M-2, U\gamma^{-1/2}) - U^4\gamma^{-2} \Gamma_{\text{up}}(M-4, U\gamma^{-1/2}). \quad (27)$$

From (25), (27) and (23) and using the fact that $M = UN_T$, we attain the closed-form NMSE expression at the intended position as in (6).

Appendix B. Appendix II

Considering a RV $Z_m = Y_{1,m} \cdot Y_{2,m}$, where $Y_{1,m} \sim \mathcal{CN}(0, \sigma_{Y_1}^2)$, $Y_{2,m} \sim \mathcal{CN}(0, \sigma_{Y_2}^2)$, and defining $R_m = |Z_m|$, $\Theta_m = \angle Z_m$, where \angle is the angle operator, the marginal joint PDF of R_m and Θ_m has been derived in [30, eq. (17)] as follows

$$f_{R_m, \Theta_m}(r_m, \theta_m) = \frac{2r_m}{\pi \sigma_{Y_1}^2 \sigma_{Y_2}^2} \mathbb{K}_0 \left(\frac{2r_m}{\sigma_{Y_1} \sigma_{Y_2}} \right). \quad (28)$$

where $\mathbb{K}_M(\cdot)$ is the M th order modified Bessel function of the second kind. The characteristic function (CF) of R_m and Θ_m can be written as

$$\begin{aligned} \psi_{R_m, \Theta_m}(j\omega_1, j\omega_2) &= \int_{-\infty}^{\infty} \int_{-\infty}^{\infty} e^{(j\omega_1 r_m \cos \theta_m + j\omega_2 r_m \sin \theta_m)} \\ &\quad \cdot f_{R_m, \Theta_m}(r_m, \theta_m) dr_m d\theta_m \\ &= \int_0^{\infty} \int_0^{2\pi} e^{(j\omega_1 r_m \cos \theta_m + j\omega_2 r_m \sin \theta_m)} d\theta_m \\ &\quad \cdot \frac{2}{\pi \sigma_{Y_1}^2 \sigma_{Y_2}^2} r_m \mathbb{K}_0 \left(\frac{2r_m}{\sigma_{Y_1} \sigma_{Y_2}} \right) dr_m \end{aligned} \quad (29)$$

Applying the equation [31, eq. (3.937-2)] to the inner integral of (29), we can obtain the following result

$$\int_0^{2\pi} e^{(j\omega_1 r_m \cos \theta_m + j\omega_2 r_m \sin \theta_m)} d\theta_m = 2\pi \mathbb{I}_0 \left(jr_m \sqrt{\omega_1^2 + \omega_2^2} \right) \quad (30)$$

where $\mathbb{I}_M(\cdot)$ is the modified Bessel function of the first kind with order M . The CF of R_m and Θ_m can be rewritten as

$$\begin{aligned} \psi_{R_m, \Theta_m}(j\omega_1, j\omega_2) &= \frac{4}{\sigma_{Y_1}^2 \sigma_{Y_2}^2} \cdot \int_0^{\infty} r_m \cdot \mathbb{I}_0 \left(jr_m \sqrt{\omega_1^2 + \omega_2^2} \right) \\ &\quad \cdot \mathbb{K}_0 \left(\frac{2r_m}{\sigma_{Y_1} \sigma_{Y_2}} \right) dr_m \end{aligned} \quad (31)$$

Using the integration formula [31, eq. (6.576-3)], we achieve the CF as follows

$$\psi_{R_m, \Theta_m}(j\omega_1, j\omega_2) = {}_2F_1 \left(1, 1; 1; -\frac{\sigma_{Y_1}^2 \sigma_{Y_2}^2 (\omega_1^2 + \omega_2^2)}{4} \right), \quad (32)$$

where ${}_2F_1(\alpha, \beta; \lambda; z)$ is the Gaussian hypergeometric function. Due to the fact that ${}_2F_1(\alpha, 1; 1; z) = (1-z)^{-\alpha}$, (32) becomes

$$\psi_{R_m, \Theta_m}(j\omega_1, j\omega_2) = \left(1 + \frac{\sigma_{Y_1}^2 \sigma_{Y_2}^2 (\omega_1^2 + \omega_2^2)}{4} \right)^{-1}. \quad (33)$$

Considering the RV $Z = \sum_{m=0}^{M-1} Z_m$ with its modulus $R = |Z|$ and its argument $\Theta = \angle Z$ and assuming that Z_m and Z_n are statistically independent for $\forall m \neq n$, the CF of R_m and Θ_m corresponding to the RV Z can be derived based on the properties of CF as follows

$$\psi_{R, \Theta}(j\omega_1, j\omega_2) = \left(1 + \frac{\sigma_{Y_1}^2 \sigma_{Y_2}^2 (\omega_1^2 + \omega_2^2)}{4} \right)^{-M}. \quad (34)$$

Inverting the CF $\psi_{R, \Theta}(j\omega_1, j\omega_2)$, we can obtain the PDF of Z . Instead of directly inverting this CF, which is a non-trivial problem, we consider the following joint PDF

$$f_{R, \Theta}(r, \theta) = \frac{2r^M}{\pi \cdot \Gamma(M) \cdot (\sigma_{Y_1} \sigma_{Y_2})^{M+1}} \mathbb{K}_{M-1} \left(\frac{2r}{\sigma_{Y_1} \sigma_{Y_2}} \right). \quad (35)$$

After carrying out the same manipulations as for $f_{R_m, \Theta_m}(r_m, \theta_m)$ (from (29) to (33)), we get the same CF as in (34). Therefore, we can conclude that $f_{R, \Theta}(r, \theta)$ function in (35) is the marginal joint PDF of the RV Z . Integrating the joint PDF over the RV θ , we obtain the PDF of $|Z|$ as in (9).

Appendix C. Appendix III

From (11) and (14), $\mathbb{K}_{M-1}(2z)$ in (10) can be approximated by

$$\mathbb{K}_{M-1}(2z) \approx \begin{cases} e^{-2z} \sum_{q=0}^D \mathbb{G}_M(q) \cdot (2z)^{q-M+1}, & \text{if } M > 1 \\ e^{-2z} \sum_{q=0}^D \mathbb{G}_1(q) \cdot (2z)^{q-2}, & \text{if } M = 1 \end{cases} \quad (36)$$

Similar to the derivation in Appendix A, we split the NMSE at the unintended position (10) into two integrals to ensure the convergence when applying the Taylor expansion. More particularly, (10) can be rewritten as

$$\begin{aligned} \text{NMSE} &\approx \frac{4}{\Gamma(M)} \int_0^{U\gamma^{-1/2}} \left(1 + \frac{z^2}{U^2\gamma^{-1}} \right)^{-1} z^M \mathbb{K}_{M-1}(2z) dz \\ &\quad + \frac{4}{\Gamma(M)} \int_{U\gamma^{-1/2}}^{\infty} U^2\gamma^{-1} \left(1 + \frac{U^2\gamma^{-1}}{z^2} \right)^{-1} z^{M-2} \mathbb{K}_{M-1}(2z) dz. \end{aligned} \quad (37)$$

Applying the Taylor series expansion to (37), we obtain the following NMSE approximation

$$\begin{aligned} \text{NMSE} &\approx \frac{4}{\Gamma(M)} \int_0^{U\gamma^{-1/2}} z^M \mathbb{K}_{M-1}(2z) dz \\ &\quad - \frac{4}{\Gamma(M) U^2\gamma^{-1}} \int_0^{U\gamma^{-1/2}} z^{M+2} \mathbb{K}_{M-1}(2z) dz \\ &\quad + \frac{4}{\Gamma(M) U^4\gamma^{-2}} \int_0^{U\gamma^{-1/2}} z^{M+4} \mathbb{K}_{M-1}(2z) dz \\ &\quad + \frac{4U^2\gamma^{-1}}{\Gamma(M)} \int_{U\gamma^{-1/2}}^{\infty} z^{M-2} \mathbb{K}_{M-1}(2z) dz \\ &\quad - \frac{4U^4\gamma^{-2}}{\Gamma(M)} \int_{U\gamma^{-1/2}}^{\infty} z^{M-4} \mathbb{K}_{M-1}(2z) dz. \end{aligned} \quad (38)$$

We derive the first integral in (38) using the approximation in (36) as follows

$$\begin{aligned} J_1 &= \frac{4}{\Gamma(M)} \int_0^{U\gamma^{-1/2}} z^M \mathbb{K}_{M-1}(2z) dz \\ &\approx \frac{4}{\Gamma(M) 2^M} \begin{cases} \int_0^{U\gamma^{-1/2}} \sum_{q=0}^D \mathbb{G}_M(q) \cdot (2z)^{q+1} \cdot e^{-2z} dz, & \text{if } M > 1 \\ \int_0^{U\gamma^{-1/2}} \sum_{q=0}^D \mathbb{G}_1(q) \cdot (2z)^{q-1} \cdot e^{-2z} dz, & \text{if } M = 1 \end{cases} \end{aligned} \quad (39)$$

By changing the variable, i.e., $x = 2z$, after some manipulations, J_1 can be derived as follows

$$J_1 \approx \begin{cases} \frac{1}{(M-1)! 2^{M-1}} \sum_{q=0}^D \mathbb{G}_M(q) \cdot \Gamma_{low}(q+2, 2U\gamma^{-1/2}), & \text{if } M > 1 \\ \sum_{q=0}^D \mathbb{G}_1(q) \cdot \Gamma_{low}(q, 2U\gamma^{-1/2}), & \text{if } M = 1 \end{cases} \quad (40)$$

Carrying out the same derivation for the four integrals left in (38), we obtain the following results

$$J_2 = \frac{4}{\Gamma(M) U^2\gamma^{-1}} \int_0^{U\gamma^{-1/2}} z^{M+2} \mathbb{K}_{M-1}(2z) dz$$

$$J_3 \approx \begin{cases} \frac{1}{U^2 \gamma^{-1} (M-1)! 2^{M+1}} \cdot \sum_{q=0}^D \mathbb{G}_M(q) \\ \quad \cdot \Gamma_{low}(q+4, 2U\gamma^{-1/2}), & \text{if } M > 1 \\ \frac{1}{4U^2 \gamma^{-1}} \sum_{q=0}^D \mathbb{G}_1(q) \cdot \Gamma_{low}(q+2, 2U\gamma^{-1/2}), \\ \quad \text{if } M = 1 \end{cases} \quad (41)$$

$$J_3 = \frac{4}{\Gamma(M) U^4 \gamma^{-2}} \int_0^{U\gamma^{-1/2}} z^{M+4} \mathbb{K}_{M-1}(2z) dz$$

$$\approx \begin{cases} \frac{1}{U^4 \gamma^{-2} (M-1)! 2^{M+3}} \cdot \sum_{q=0}^D \mathbb{G}_M(q) \cdot \Gamma_{low}(q+6, 2U\gamma^{-1/2}), \\ \quad \text{if } M > 1 \\ \frac{1}{16U^4 \gamma^{-2}} \sum_{q=0}^D \mathbb{G}_1(q) \cdot \Gamma_{low}(q+4, 2U\gamma^{-1/2}), \\ \quad \text{if } M = 1 \end{cases} \quad (42)$$

$$J_4 = \frac{4U^2 \gamma^{-1}}{\Gamma(M)} \int_{U\gamma^{-1/2}}^{\infty} z^{M-2} \mathbb{K}_{M-1}(2z) dz$$

$$\approx \begin{cases} \frac{U^2 \gamma^{-1}}{(M-1)! 2^{M-3}} \sum_{q=0}^D \mathbb{G}_M(q) \cdot \Gamma_{up}(q, 2U\gamma^{-1/2}), \\ \quad \text{if } M > 1 \\ 4U^2 \gamma^{-1} \sum_{q=0}^D \mathbb{G}_1(q) \cdot \Gamma_{up}(q-2, 2U\gamma^{-1/2}), \\ \quad \text{if } M = 1 \end{cases} \quad (43)$$

and

$$J_5 = \frac{4U^4 \gamma^{-2}}{\Gamma(M)} \int_{U\gamma^{-1/2}}^{\infty} z^{M-4} \mathbb{K}_{M-1}(2z) dz$$

$$\approx \begin{cases} \frac{U^4 \gamma^{-2}}{(M-1)! 2^{M-5}} \sum_{q=0}^D \mathbb{G}_M(q) \cdot \Gamma_{up}(q-2, 2U\gamma^{-1/2}), \\ \quad \text{if } M > 1 \\ 16U^4 \gamma^{-2} \sum_{q=0}^D \mathbb{G}_1(q) \cdot \Gamma_{up}(q-4, 2U\gamma^{-1/2}), \\ \quad \text{if } M = 1 \end{cases} \quad (44)$$

Due to the fact that $M = UN_T$, $\Gamma(M) = (M-1)!$ for a positive integer M , substituting (40), (41), (42), (43) and (44) into (38) yields the closed-form NMSE approximation as in (13).

References

- [1] Y. Chen, Y.-H. Yang, F. Han, K.J.R. Liu, Time-reversal wideband communications, *IEEE Signal Process. Lett.* 20 (12) (2013) 1219–1222.
- [2] M. Emami, M. Vu, J. Hansen, A.J. Paulraj, G. Papanicolaou, Matched filtering with rate back-off for low complexity communications in very large delay spread channels, in: *Proc. Conf. Record 38th Asilomar Conf. Signals Syst. Comput.*, Vol. 1, 2004, pp. 218–222.
- [3] T.-H. Nguyen, S. Monfared, J.-F. Determe, J. Louveaux, P. De Doncker, F. Horlin, Performance analysis of frequency domain precoding time-reversal MISO OFDM systems, *IEEE Commun. Lett.* 24 (1) (2020) 48–51.
- [4] T.-C. Wu, Y.-C. Chi, H.-Y. Wang, C.-T. Tsai, G.-R. Lin, Blue laser diode enables underwater communication at 12.4 Gbps, *Sci. Rep.* 7 (2017) Article # 40480.
- [5] Y.-F. Huang, C.-T. Tsai, Y.-C. Chi, D.-W. Huang, G.-R. Lin, Filtered multicarrier OFDM encoding on blue laser diode for 14.8-Gbps seawater transmission, *IEEE J. Lightw. Technol.* 36 (9) (2018) 1739–1745.
- [6] T. Dubois, M. Helard, M. Crussiere, C. Germond, Performance of time reversal precoding technique for MISO-OFDM systems, *EURASIP J. Wireless Commun. Networking* 260 (2013) article # 2013.

- [7] T.-H. Nguyen, M. Va. Eeckhaute, J.-F. Determe, J. Louveaux, P. De Doncker, F. Horlin, Analysis of residual CFO impact on downlink massive MISO systems, *IET Electron. Lett.* 55 (18) (2019) 1017–1019.
- [8] M. Fink, Acoustic time-reversal mirrors, in: M. Fink, W. Kuperman, J.-P. Montagner, A. Tourin (Eds.), *Imaging of Complex Media with Acoustic and Seismic Waves*, in: *Topics in Applied Physics*, vol. 84, Springer Berlin Heidelberg, 2002.
- [9] B. Bogert, Demonstration of delay distortion correction by time-reversal techniques, *IRE Trans. Commun. Syst.* 5 (3) (1957) 2–7.
- [10] F. Amoroso, Optimum realizable transmitter waveforms for high-speed data transmission, *IEEE Trans. Commun. Technol.* 14 (1) (1966) 8–13.
- [11] M. Fink, C. Prada, F. Wu, D. Cassereau, Self focusing in inhomogeneous media with time reversal acoustic mirrors, in: *Proceedings of Ultrasonics Symposium*, Vol. 2, 1989, pp. 681–686.
- [12] A.J. Devaney, Time reversal imaging of obscured targets from multi-static data, *IEEE Trans. Antennas Propag.* 53 (5) (2005) 1600–1610.
- [13] Y. Jin, J.M.F. Moura, Time-reversal detection using antenna arrays, *IEEE Trans. Signal Process.* 57 (4) (2009) 1396–1414.
- [14] Y. Chen, B. Wang, Y. Han, H.Q. Lai, Z. Safar, K.J.R. Liu, Why time reversal for future 5g wireless? [perspectives], *IEEE Signal Process. Mag.* 33 (2) (2016) 17–26.
- [15] Q. Xu, P. Ren, Q. Du, L. Sun, Security-aware waveform and artificial noise design for time-reversal-based transmission, *IEEE Trans. Veh. Technol.* 67 (6) (2018) 5486–5490.
- [16] Z.-H. Wu, Y. Han, Y. Chen, K.J.R. Liu, A time-reversal paradigm for indoor positioning system, *IEEE Trans. Veh. Technol.* 64 (4) (2015) 1331–1339.
- [17] T.-H. Nguyen, J. Louveaux, P. De Doncker, F. Horlin, Impact of I/Q imbalance on time reversal-based indoor positioning systems, in: *IEEE 14th International Conference on Wireless and Mobile Computing, Networking and Communications, WiMob*, 2018, pp. 36–41.
- [18] T.-H. Nguyen, S. Golstein, J. Louveaux, P. De Doncker, F. Horlin, Performance analysis and mitigation method for I/Q imbalance-impaired time reversal-based indoor positioning systems, in: *IEEE 90th Vehicular Technology Conference, VTC2019-Fall*, 2019, Sep.
- [19] Q. Xu, Y. Chen, B. Wang, K.J.R. Liu, TRIEDS: Wireless events detection through the wall, *IEEE Internet Things J.* 4 (3) (2017) 723–735.
- [20] C. Chen, Y. Han, Y. Chen, H.Q. Lai, F. Zhang, B. Wang, K.J.R. Liu, TR-BREATH: Time-reversal breathing rate estimation and detection, *IEEE Trans. Biomed. Eng.* 65 (3) (2018) 489–501.
- [21] M. Speth, S. Fechtel, G. Fock, H. Meyr, Optimum receiver design for wireless broad-band systems using OFDM - Part I, *IEEE Trans. Commun.* 47 (11) (1999) 1668–1677.
- [22] A. Papoulis, *Probability, Random Variables and Stochastic Processes*, third ed., McGraw-Hill Companies, 1991.
- [23] M.M. Mollu, P. Xiao, M. Khalily, L. Zhang, R. Tafazolli, A novel equivalent definition of modified Bessel functions for performance analysis of multi-hop wireless communication systems, *IEEE Access* 5 (2017) 7594–7605.
- [24] <https://functions.wolfram.com/Bessel-TypeFunctions/BesselK/>, (Access on 10th Jan. 2019).
- [25] NIST Digital Library of Mathematical Functions, link: <https://dlmf.nist.gov/>
- [26] 3GPP - TS 36.101, User equipment (UE) radio transmission and reception, in: 3rd Generation Partnership Project; Technical Specification Group Radio Access Network; Evolved Universal Terrestrial Radio Access, E-UTRA, 2017, URL: <http://www.3gpp.org>.
- [27] S. Alizadeh, H.K. Bizaki, M. Okhovvat, Effect of channel estimation error on performance of time reversal-UWB communication system and its compensation by pre-filter, *IET Commun.* 6 (12) (2012) 1781–1794.
- [28] E. Bjornson, J. Hoydis, L. Sanguinetti, Massive MIMO has unlimited capacity, *IEEE Trans. Wirel. Commun.* 17 (1) (2018) 574–590.
- [29] P. Duhamel, M. Vetterli, Fast fourier transforms: a tutorial review and a state of the art, *Signal Process.* 19 (4) (2003) 259–299.
- [30] N. O'Donoghue, J.M.F. Moura, On the product of independent complex Gaussians, *IEEE Trans. Signal Process.* 60 (3) (2012) 1050–1063.
- [31] I.S. Gradshteyn, I.M. Ryzhik, *Tables of Integrals, Series and Products*, seventh ed., San Diego Academic, 2007.



Trung-Hien Nguyen received the B.Sc. degree in electronics and telecommunications from the Hanoi Posts and Telecommunications Institute of Technology (PTIT), Vietnam, in 2010 and the Ph.D. degree in physics from the University of Rennes 1, France, in 2015. His thesis was carried out within the Fonctions optiques pour les technologies de l'information (FOTON) Laboratory, CNRS, in Lannion, France. Since December 2015, he has been with the OPERA department, Université libre de Bruxelles (ULB), Belgium, as a postdoctoral researcher. His research interests are in the fields of optical fiber communication systems (with an emphasis on advanced modulation formats and digital signal processing) and of localization based on 5G signals.



Jean-François Determe received the electrical engineering degree (Master en ingénieur civil électricien) from Université libre de Bruxelles (ULB) in 2013. He also received the Ph.D. in Engineering jointly from ULB and Université catholique de Louvain in 2018. From 2013 to 2017, he was an FNRS research fellow, funded by the Belgian FRS-FNRS. Since 2018, he has been a postdoctoral researcher with the OPERA-WCG department at ULB.



Shaghayegh Monfared received the M.Sc. degree in Telecommunication Engineering from Imam Khomeini International University (IKIU), Iran, in 2012 and she joined in Huawei Technologies as a Service Management Engineer. From 2015 to 2017, she worked at the Department of Computer Science and Engineering, University of Lisbon. Since then she is a Ph.D. researcher at OPERA WCG, Université libre de Bruxelles and her research is mainly focused on the design and prototyping of the localization systems for Internet-of-Thing (IoT) networks.



Jerome Louveaux received the electrical engineering degree and the Ph. D. degree from the Université catholique de Louvain (UCL), Louvain-la-Neuve, Belgium in 1996 and 2000 respectively. From 2000 to 2001, he was a visiting scholar in the Electrical Engineering department at Stanford University, CA. From 2004 to 2005, he was a postdoctoral researcher at the Delft University of technology, Netherlands. Since 2006, he has been a Professor in the ICTEAM institute at UCL. His research interests are in signal processing for digital communications, and in particular: multicarrier

modulations, xDSL systems, resource allocation, synchronization and estimation. Prof. Louveaux was a co-recipient of the "Prix biennal Siemens 2000" for a contribution on filter-bank based multi-carrier transmission and co-recipient of the "Prix Scientifique Alcatel 2005" for a contribution in the field of powerline communications.



Philippe De Doncker received the M.Sc. degree in physics engineering and the Ph.D. degree in science engineering from the Université Libre de Bruxelles (ULB), Brussels, Belgium, in 1996 and 2001, respectively. He is currently a Professor with the ULB, where he leads the research activities on wireless channel modeling and electromagnetics.



François Horlin received the Ph.D. degree from the Université catholique de Louvain (UCL) in 2002. He specialized in the field of signal processing for digital communications. After his Ph.D., he joined the Inter-university Micro-Electronics Center (IMEC). He led the project aiming at developing a 4G cellular communication system in collaboration with Samsung Korea. In 2007, François Horlin became professor at the Université libre de Bruxelles (ULB). He is currently supervising a research team working on next generation communication systems. Localization based on 5G signals, filterbank-based modulations, massive MIMO and dynamic spectrum access are examples of currently investigated research topics.